Preprint
2021

APPLICATION OF HYBRID URANS/DVMS AND DDES/DVMS METHODS TO FLOW AROUND CYLINDERS

Stephen Wornom(*), Florian Miralles(*), Bruno Koobus(*), Alain Dervieux(**)

(*)IMAG, Université de Montpellier, 34090 Montpellier, France, stephen.Wornom@inria.fr, florian.miralles@umontpellier.fr, bruno.koobus@umontpellier.fr,
(**)Société LEMMA, 2000 route des Lucioles, Sophia-Antipolis, France, and Université Côte d'Azur/INRIA, 2004 Route des lucioles, 06902 Sophia-Antipolis, France, alain.dervieux@inria.fr

Abstract: This paper studies the influence of LES and hybrid models on vortex shedding around cylinders with a focus on three Reynolds numbers, namely 140K, 1M, 2M. Several existing and new hybrid models are compared. This work takes place in the Norma project partly supported by the French National Research Agency.
Keywords: unstructured mesh, finite volume, hybrid turbulence models, LES, DES, circular cylinder.

1 Introduction

The paper studies the influence of LES and hybrid models on vortex shedding with an emphasis on noise generation for aeroacoustic calculations. High-fidelity Aeroacoustics models the creation of noise in unstable turbulent parts of a flow. For this purpose, the models need to behave like Large-Eddy Simulation (LES) models. Large Eddy Simulation is able to describe turbulent boundary layers on a quasi-direct simulation mode, with extremely fine discretizations. At the same time, Aeroacoustics has the ambition to address complex industrial flows, of high Reynolds number, involving very thin boundary layers, which today's computers and software cannot compute on a LES mode, only on a RANS mode. To account for both needs, LES and RANS, the hybrid model approach, combining LES and RANS in a somewhat zonal way is considered by many research teams.
After a seminal paper by C. Speziale [28], an important contribution was the proposition of the DES method, [27]. This method, initally based on the Spalart-Allmaras one-equation closure has been used and extended by many teams, and notably to the SST-$k-\omega$.
Hybrid models are important models for aeroacoustics, assumed to be rather good LES models. They are useful for the high Reynolds flows of aeronautics, allowing a rather good prediction of the vortices which generate noise. Even for low Reynolds flow, they can appear as better than RANS, while not being completely satisfactory.
Engineering problems involve more and more complex geometries with details around which global flows are both of high Reynolds and low Reynolds. Details can involve blunt bodies like landing gears, antennas, can involve after bodies, or shapes that can be far from aerodynamic thin shapes (e.g. multi-rotor drones). A typical geometry to study to try to better address this issue is the massively separated flow past a circular cylinder at rather high Reynolds numbers.

In this paper, we review a few hybrid turbulence models in combination with two numerical schemes. We compare them on a benchmark of cylinder flows and a typical aeroacoustic flow in order to examine the relation between pure LES abilities and aeroacoustic ones. The hybrid methods look like:

$$Hybrid = URANS \times \theta + LES \times (1 - \theta)$$

where θ is a blending function. The main sections of this report examine several blending functions proposed in the literature and a geometric blending function proposed in this thesis. The plan is as follows: A first part presents the numerical scheme. A second part presents the different turbulence models which will be computed. A third part compares results on the cylinders.

2 Numerical modeling

The numerical approach which is selected is basically a second-order accurate vertex centered approximation. Dual cells are limited by facets, which are triangles, each of them being formed by a mid-edge, a centroid of face, a centroid of tetraedron, Figure 1. The assemby of fluxes is edge based. For each edge ij of the mesh fluxes are computed through the union of facets being the common boundary between two dual cells around the vertices i and j.

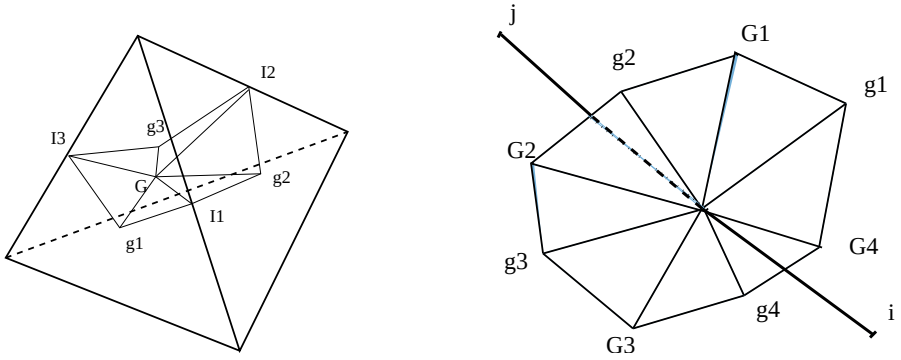

Figure 1: left, intersection of the boundary of a cell with a tetrahedron. Right, intersection of the boundaries of cell i and cell j, on the facet of which is integrated the flux between Cell i and cell j.

The flux between each couple (i,j) of cells is numerically integrated through a unique approximate Riemann solver $\mathrm{ARS}(W_{ij}, W_{ji}, \nu_{ij})$. The integration values W_{ij} W_{ji} are two special upwind and downwind interpolations of the unknown field W located at the middle I_{ij} of the edge ij. For these interpolations, we consider two methods, each of them resulting in a superconvergent approximation. By superconvergence we mean that for some Cartesian meshes, the accuracy may be much higher the second-order. The purpose is not higher-order convergence in this particular context but a strong reduction of dissipation and some reduction of the dispersion in the general case of a non-Cartesian but not so irregular mesh as generated for our aeroacoustic calculations.

For cell-interface reconstruction, the V6 scheme has been introduced in [4, 2]. The interpolation W_{ij} uses the value of the field and its gradient on vertex j and on the vertices of the upwind tetrahedron T_{ij}. The interpolation W_{ji} uses the value of the field and its gradient on vertex i and on the vertices of the downwind tetrahedron T_{ji}, Figure 2. The scheme is fifth-order accurate on certain Cartesian meshes, and is (solely) stabilized by a sixth-order dissipation the strength

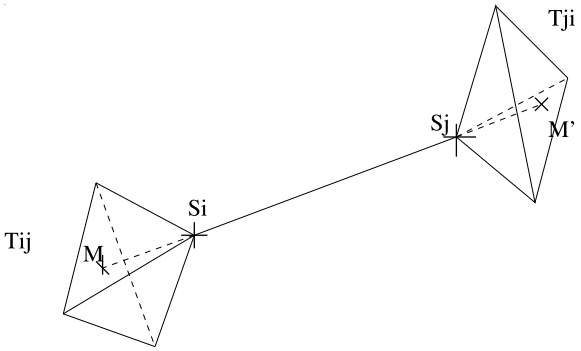

Figure 2: Butterfly molecule in 3D: Downwind and Upwind tetrahedra are tetrahedra having respectively S_i and S_j as a vertex and such that line S_iS_j intersects the opposite face.

of which can be tuned by a parameter $\gamma \in]0,1]$ (see [4, 2] for details).

3 Two equation RANS modeling

3.1 Goldberg model

The Goldberg-Peroomian-Chakravarthy [10] low Reynolds $k-\varepsilon$ model has the following interesting features : (1) a wall-distance-free model, (2) a good prediction of flows with adverse pressure gradient, (3) a good ability to predict separated flows and is then a low Reynolds model suitable for the simulation of blunt body flows in which we are interested. We describe it now for completeness in a short manner. First, the turbulent viscosity is written:

$$\mu_t = c_\mu f_\mu \rho \frac{k^2}{\varepsilon} \quad \text{with} \quad f_\mu = \frac{1-e^{-A_\mu R_t}}{1-e^{-R_t^{1/2}}} max(1, \psi^{-1}),$$
$$c_\mu = 0.09 \ , \ A_\mu = 0.01 \ , \ \psi = R_t^{1/2}/C_\tau$$

and $R_t = k^2/(\nu\varepsilon)$ with $\nu = \mu/\rho \quad ; \quad C_\tau = 1.41$. The closure variables are determined by:

$$\begin{aligned}
\frac{\partial \overline{\rho} k}{\partial t} + \frac{\partial (\overline{\rho}\widetilde{v}_j k)}{\partial x_j} &= \frac{\partial \Big[\Big(\mu + \frac{\mu_t}{\sigma_k}\Big)\frac{\partial k}{\partial x_j}\Big]}{\partial x_j} + \tau_{ij}\frac{\partial \widetilde{v}_i}{\partial x_j} - \overline{\rho}\varepsilon \\
\frac{\partial \overline{\rho} \varepsilon}{\partial t} + \frac{\partial (\overline{\rho}\widetilde{v}_j \varepsilon)}{\partial x_j} &= \frac{\partial \Big[\Big(\mu + \frac{\mu_t}{\sigma_\varepsilon}\Big)\frac{\partial \varepsilon}{\partial x_j}\Big]}{\partial x_j} + \Big(C_{\varepsilon 1}\tau_{ij}\frac{\partial \widetilde{v}_i}{\partial x_j} - C_{\varepsilon 2}\overline{\rho}\varepsilon + E\Big)T_\tau^{-1}
\end{aligned}$$

where $C_{\varepsilon 1} = 1.42$,$C_{\varepsilon 2} = 1.83$ and $T_\tau = \frac{k}{\varepsilon} max(1, \psi^{-1})$ is the realisable time scale ($\tau = k/\varepsilon$). Furthermore,

$$E = \rho A_E max(\sqrt{k},\ (\nu\varepsilon)^{0.25})(\varepsilon T_\tau)^{0.5} max(\frac{\partial k}{\partial x_i}\frac{\partial \tau}{\partial x_i},\ 0)$$

with $A_E = 0.3$. This model solves indeed the flow up to the wall but in some case it can be useful to couple it with a *Reichardt wall law*:

$$U^+ = \frac{1}{\kappa}\ln\left(1+\kappa y^+\right) + 7.8\left[1 - \exp\left(\frac{-y^+}{11}\right) - \frac{-y^+}{11}\exp\left(\frac{-y^+}{3}\right)\right] \tag{1}$$

Since the Goldberg model is a low-Reynolds one, the matching thickness can be arbitrarily small.

Menter correction

The Menter correction, which limits the eddy viscosity when production is greater than dissipation, has the good following features : (1) it reduces the eddy viscosity in non-equilibrium flows and therefore improves the ability of the model to predict separated flows, (2) it limits the generation of turbulence in impingement zones (which is excessive with classic RANS model). It is then appropriate to blunt body flow computation.

The previous definition of μ_t is replaced by:

$$\mu_t = \frac{\rho k \sqrt{c_\mu f_\mu}}{max\left(\frac{\varepsilon}{k\sqrt{c_\mu f_\mu}}, \mid \frac{\partial u}{\partial y} \mid tanh(\psi^2)\right)} \quad \text{with} \quad \psi = max\left(2\frac{k^{3/2}}{y\varepsilon}, \frac{500\mu c_\mu k}{\rho\varepsilon y^2 Re}\right).$$

It has been remarked, for example in ([7]) that the combination of a $k-\varepsilon$ with the above Menter limiter carried a favourable behavior, somewhat similar to the $k-\omega$ SST model. We denote in the sequel the association of Goldberg's closure with Menter's limiter as the *RANS* $k-\varepsilon$*-Menter* model and write it in short:

$$\Big(\frac{\partial \langle W\rangle}{\partial t}, \phi_i\Big) + (\nabla \cdot F(\langle W\rangle), \phi_i) = -\big(\tau^{RANS}(\langle W\rangle), \phi_i\big).$$

4 Dynamic Variational Multiscale modeling

The VMS formulation consists in splitting between the large resolved scales (LRS) i.e. those resolved on a virtual coarser grid, and the small resolved ones (SRS) which correspond to the finest level of discretization. The VMS-LES method does not compute the SGS component of the solution, but it models its dissipative effects on the SRS, and it preserves the Navier-Stokes model for the large resolved scales.

4.1 VMS formulation

In the present work, we adopt the VMS approach proposed in [18] for the simulation of compressible turbulent flows through a finite volume/finite element discretization on unstructured tetrahedral grids. Let V_{FV} be the space spanned by ψ_k, the finite volume basis function, and V_{FE} the one spanned by ϕ_k, the finite element basis function. In order to separate large and small scales, these spaces are decomposed as: $\psi_k =< \psi_k > +\psi'_k$ and $\phi_k =< \phi_k > +\phi'_k$ where the *brackets* denote a coarse scale and the *prime* a fine scale. Consequently to this decomposition, the flow variables are decomposed as follows:

$$W =< W > +W' + W^{SGS} \tag{2}$$

where $< W >$ are the LRS, W' the SRS and W^{SGS} the unresolved scales. The projection operator based on spatial average on macro-cells defined in [18] is used to compute the basis functions of the LRS space. This, for finite elements, leads to:

$$< \phi_k >= \frac{Vol(C_k)}{\sum_{j\epsilon I_k} Vol(C_j)} \sum_{j\epsilon I_k} \phi_j \tag{3}$$

where $Vol(C_j)$ denotes the volume of C_j, the cell around the vertex j, and $I_k = \{ j/C_j \in C_{m(k)} \}$ where $C_{m(k)}$ is the macro-cell containing the cell C_k. The macro-cells are obtained by a process known as agglomeration [19]. An analogous definition holds for finite-volume basis functions. The SGS model which introduces the dissipative effect of the unresolved scales on the resolved scales is only added to the SRS and it is computed only as a function of the SRS. Therefore, the term below is added to the momentum equations

$$\int_\Omega \tau' \cdot \nabla \Phi' \; d\Omega \tag{4}$$

The SGS stress tensor is expressed herein by means of an eddy-viscosity model and, as previously stated, it is computed as a function of the small resolved scales:

$$\tau'_{ij} = -\mu'_{sgs}(2S'_{ij} - \frac{2}{3}S'_{kk}\delta_{ij}) \; ; \quad S'_{ij} = \frac{1}{2}(\frac{\partial u'_i}{\partial x_j} + \frac{\partial u'_j}{\partial x_i}) \tag{5}$$

where μ'_{sgs} denotes the viscosity of the SGS model used to close the problem, computed as a function of the smallest resolved scales, and u'_i is the i-th component of the SRS velocity. Likewise, the term

$$\int_\Omega \frac{C_p \mu'_{sgs}}{Pr_{sgs}} \nabla T' \cdot \nabla \Phi'_5 \; d\Omega \tag{6}$$

is added to the energy equation. C_p is the specific heat at constant pressure, Pr_{sgs} is the subgrid-scale Prandtl number which is assumed to be constant and T' the SRS temperature.

4.2 SGS viscosities

To obtain the SGS viscosity needed to close the above VMS formulation, we have to define the SGS viscosity coefficient μ'_{sgs}.

A first option is the widely used Smagorinsky model [26] is first considered. In the adopted VMS formulation this writes:

$$\mu'_{\rm sgs} = < \rho > (C_{\rm S}\Delta)^2 \left|S'\right| \quad , \quad \text{with} \quad \left|S'\right| = \sqrt{2S'_{ij}S'_{ij}} \tag{7}$$

where $C_{\rm S}$ is the Smagorinsky coefficient A typical value for the Smagorinsky coefficient for shear flows is $C_{\rm S} = 0.1$, which is used herein.

Symbol Δ holds for the *filter width*, in the type of LES which we use, the filter width is fixed to the *local mesh size*. The definition of the local mesh size is not an easy question when (highly) anisotropic meshes are used. Two main options are (1) the third root of the grid element volume and (2) the largest local edge. However, our experience is that, when combined with devices like VMS and Dynamic-LES, the choice in defining the local mesh size is not so sensitive. Our filter width is defined as the third root of volume of the grid element T, then:

$$\Delta \; = \; \Delta_T \; = \; \big(\int_T {\rm d}v \big)^{\frac{1}{3}}. \tag{8}$$

Symbol Δ holds for the *filter width*, in the type of LES which we use, the filter width is fixed to the *local mesh size*. The definition of the local mesh size is not an easy question when (highly) anisotropic meshes are used. Two main options are (1) the third root of the grid element volume and (2) the largest local edge. However, our experience is that, when combined with devices like VMS and Dynamic-LES, the choice in defining the local mesh size is not so sensitive. Our filter width is defined as the third root of volume of the grid element T, then:

$$\Delta \;=\; \Delta_T \;=\; \big(\int_T \mathrm{d}v\big)^{\frac{1}{3}}. \tag{9}$$

A second SGS model is the Wall-Adapting Local Eddy -Viscosity (WALE) SGS model proposed by Nicoud and Ducros [21]. The eddy-viscosity term in the VMS formulation is defined as follows:

$$\mu'_{\mathrm{sgs}} = <\rho>(C_W\Delta)^2\frac{((S^d_{ij})'(S^d_{ij})')^{\frac{3}{2}}}{(S'_{ij}S'_{ij})^{\frac{5}{2}}+((S^d_{ij})'(S^d_{ij})')^{\frac{5}{4}}} \tag{10}$$

with $(S^d_{ij})' = \frac{1}{2}({g'_{ij}}^2+{g'_{ji}}^2)-\frac{1}{3}\delta_{ij}{g'_{kk}}^2$ being the symmetric part of the tensor ${g'_{ij}}^2 = g'_{ik}g'_{kj}$, where $g'_{ij} = \partial u'_i/\partial x_j$. As indicated in [21], the constant C_W is set to 0.5.

4.3 Dynamic model

In their original formulations, C_{S} and C_W appearing in the expression of the viscosity of the Smagorinsky and WALE SGS model (Eqs. (7) and (10) respectively) are set to a constant over the entire flow field and in time. In the dynamic model [8], this constant is replaced by a dimensionless parameter $C(x,t)$ that is allowed to be a function of space and time. The dynamic approach also provides a systematic way for adjusting this parameter in space and time by using information from the resolved scales. After the introduction of the grid filter, denoted by *overline* and *tilde*, *tilde* being Favre averaging, $\tilde{f} = \overline{\rho f}/\overline{\rho}$, a second filter is considered, having a larger width than the grid one, which is called the test-filter and denoted by a *hat*. The test-filter is applied to the grid-filtered Navier-Stokes equations, and then, the subtest-scale stress is defined as follows:

$$M^{test}_{ij} = \widehat{\overline{\rho}\overline{\mathbf{u}_i}\overline{\mathbf{u}_j}} - \big(\hat{\overline{\rho}}\big)^{-1}\left(\widehat{\overline{\rho}\overline{\mathbf{u}_i}}\;\widehat{\overline{\rho}\overline{\mathbf{u}_i}}\right) \tag{11}$$

The deviatoric part of M^{test}_{ij} can be written using a Smagorinsky or WALE model, as

$$M^{test}_{ij} - \frac{1}{3}M^{test}_{kk}\delta_{ij} \;=\; -C\hat{\Delta}^2\hat{\overline{\rho}}g(\hat{\tilde{\mathbf{u}}})\hat{\tilde{P}}_{ij} \qquad (C \;=\; {C_W}^2 \text{ or } {C_{\mathrm{S}}}^2) \tag{12}$$

with $\hat{\tilde{P}}_{ij} \;=\; -\frac{2}{3}\hat{\tilde{S}}_{kk}\delta_{ij} + 2\hat{\tilde{S}}_{ij}$ and where $g(\hat{\tilde{\mathbf{u}}})$ denotes the contribution to the SGS viscosity depending on the gradient velocity that appears in (7) for the Smagorinsky model, and in (10) for the WALE model. The constant C, as originally proposed in [8], is assumed to be constant at the subgrid and subtest levels.

By using the Germano identity [8] and a least-square approach [20] to contract the resulting tensorial equation, we obtain:

$$(C\Delta^2) = \frac{L_{ij}B_{ij}}{B_{pq}B_{pq}} \tag{13}$$

where:

$$L_{ij} = \mathcal{L}_{ij} - \frac{1}{3}\mathcal{L}_{kk}\delta_{ij}\;; \qquad \mathcal{L}_{ij} = \widehat{\overline{\rho}\tilde{\mathbf{u}}_i\tilde{\mathbf{u}}_j} - \big(\hat{\overline{\rho}}\big)^{-1}\left(\widehat{\overline{\rho}\tilde{\mathbf{u}}_i}\widehat{\overline{\rho}\tilde{\mathbf{u}}_i}\right) \tag{14}$$

and

$$B_{ij} \;=\; \bar{\rho}\widehat{g(\tilde{\mathbf{u}})\tilde{\bar{P}}_{ij}} - \left(\frac{\hat{\Delta}}{\Delta}\right)^2 \hat{\bar{\rho}}g(\hat{\tilde{\mathbf{u}}})\hat{\tilde{\bar{P}}}_{ij}. \tag{15}$$

Note that all quantities in the right-hand side of Eq. (13) are known from the LES computation. Note also that we preferred to dynamically compute $(C\Delta^2)$, instead of C as done in the original dynamic procedure, in order to partially overcome difficulties in the definition of the filter width for inhomogeneous and unstructured grids. Finally, as done also in [14], the classical dynamic procedure previously briefly outlined, which involves all the resolved scales, is used herein. Once $(C\Delta^2)$ is dynamically computed, it is injected in Eq. (7) or (10) to obtain the SGS viscosity used in the VMS approach.

A possible drawback of the dynamic procedure based on the Germano-identity [8] when applied to a SGS model already having a correct near-wall behavior, as the WALE one, is the introduction of a sensitivity to the additional filtering procedure. A simple way to avoid this inconvenient is to have a sensor able to detect the presence of the wall, without a priori knowledge of the geometry, so that the dynamic SGS model adapts to the classical constant of the model, which is equal to 0.5 in the near wall region for the WALE model, and compute the constant dynamically otherwise. We adopt the sensor proposed in [30], having the following expression:

$$SVS = \frac{(\widetilde{S_{ij}}^d \widetilde{S_{ij}}^d)^{\frac{3}{2}}}{(\widetilde{S_{ij}}^d \widetilde{S_{ij}}^d)^{\frac{3}{2}} + (\widetilde{S_{ij}}\widetilde{S_{ij}})^3}. \tag{16}$$

This parameter has the properties to behave like y^{+3} near a solid wall, to be equal to 0 for pure shear flows and to 1 for pure rotating flows.

It should be noticed that the implementation of the dynamic SGS models in our software has been optimized so that the additional cost of the resulting dynamic LES and VMS models, in the case of an implicit time-marching scheme, which is our default option, is less than 1% compared to their non-dynamic counterparts.

5 DDES-k-eps-Menter

The above k-eps-Menter RANS can been injected in a DDES formulation in a similar way to [1], [11]. The DDES/$k-\varepsilon$ model is obtained by replacing, in the ρk transport equation of the Goldberg $k-\varepsilon$ model, the dissipation term $\rho\varepsilon$ by a DDES dissipation $\rho k^{3/2}/l_{DDES}$ introducing the characteristic length l_{DDES}:

$$\frac{\partial \bar{\rho}k}{\partial t} + \frac{\partial(\bar{\rho}\widetilde{v}_j k)}{\partial x_j} = \frac{\partial\left[\left(\mu + \frac{\mu_t}{\sigma_k}\right)\frac{\partial k}{\partial x_j}\right]}{\partial x_j} + \tau_{ij}\frac{\partial \widetilde{v}_i}{\partial x_j} - \bar{\rho}\frac{k^{3/2}}{l_{DDES}} \tag{17}$$

$$\text{where} \quad l_{DDES} = \frac{k^{3/2}}{\varepsilon} - f_d * max(0, \frac{k^{3/2}}{\varepsilon} - C_{DDES}\Delta) \tag{18}$$

$$\text{with} \quad f_d = 1 - tanh((8r_d)^3) \quad \text{and} \quad r_d = \frac{\nu_t + \nu}{max(\sqrt{u_{i,j}u_{i,j}}, 10^{-10})K^2 d_w^2}. \tag{19}$$

K denotes the von Kàrmàn constant ($K = 0.41$), d_w is the normal distance to the wall, $u_{i,j}$ is the derivative according to x_j of the component i of the velocity u, and the model constant C_{DDES} is set to the value 0.65 (ν_t and ν are the turbulent kinematic viscosity and the fluid kinematic viscosity, respectively).

$$\Big(\frac{\partial \langle W\rangle}{\partial t}, \phi_i\Big) + (\nabla \cdot F(\langle W\rangle), \phi_i) = -\big(\tau^{DDES}(\langle W\rangle), \phi_i\big),$$

in which the above RANS model is introduced in a DDES formulation by replacing in the RHS of the k equations the $D_k^{RANS} = \rho\varepsilon$ dissipation term by $D_k^{DDES} = \rho k^{\frac{3}{2}}/l_{DDES}$ with $l_{DDES} = k^{\frac{3}{2}}/\varepsilon - f_d\ max\big(0, k^{\frac{3}{2}}/\varepsilon - C_{DDES}\ \Delta\big)$ where $C_{DDES} = 0.65$. We have checked in [15] that this model gives predictions close to other DDES approach based on the $k-\omega$ SST model.

6 Further hybridation

6.1 DVMS and Hybrid DVMS

In the VMS approach [6] which we use, the effect of unresolved structures are only modeled in the equations governing the small resolved scales. In that sens the subgrid-scale is acting only on small scales and is computed by applying Smagorinsky or Wale model. We detailled briefly the VMS formulation which is semi-discretized :

$$\left\{ \begin{array}{rcl} \Big(\frac{\partial \overline{W}}{\partial t}, \chi_i\Big) + \big(\nabla \cdot F_c(\overline{W}), \chi_i\big) & = & \big(\nabla \cdot F_v(\overline{W}), \phi_i\big) + \Big(\tau^{DVMS}(W^{'}), \phi_i^{'}\Big) \\ Q(0, \mathbf{x}) & = & Q_0(\mathbf{x}), \quad \forall \mathbf{x} \in \Omega_f \end{array} \right. \tag{20}$$

Here the convective and viscous flux do not contains any closure equations. Moreover, the closure terms is defined as the following :

$$\Big(\tau^{les}(W_h^{'}), \phi_i^{'}\Big) := \big(0,\ \mathbf{M}_S(W_h, \phi_i'),\ M_H(W_h, \phi_i')\big)^T \tag{21}$$

and

$$\mathbf{M}_S(W_h, \phi_i') := \sum_{T\in\Omega_h} \int_T \rho_h (\mathcal{C}_s \Delta_T)^2 |S'| \mathcal{D}(S') \nabla \phi_i' d\mathbf{x} \tag{22}$$

here $|S'| = \sqrt{S' : S'}$, Δ_T is the local mesh size defined in (9), $\mathcal{D}(S')$ correspond to the deviatoric part of tensor $S' = \frac{1}{2}(\nabla u' + (\nabla u')^T)$ defined by $\mathcal{D}(S') = 2\big(S' - \frac{1}{3}\nabla \cdot u' Id\big)$. The basis function are written as $\phi_k' = \phi_k - \overline{\phi}_k$ where :

$$\overline{\phi}_k = \frac{Vol(C_k)}{\sum_{j\in\mathfrak{I}_k} Vol(C_j)} \sum_{j\in\mathfrak{I}_k} \phi_j \tag{23}$$

$\mathfrak{I}_k$ means the index set of cells wich are contains in macro-cell $\mathfrak{C}_k$ obtained by agglomeration process, see also [19]. For the subgrid terms in relation with heat transfer, we write :

$$M_H(W_h, \phi_i') = \sum_{T\in\Omega_h} \int_T \rho_h \frac{C_p (C_s \Delta_T)^2}{Pr_t} |S'| \nabla T' \cdot \nabla \phi_i' d\mathbf{x} \tag{24}$$

URANS/DVMS model

Now, let us define the hybrid URANS/DVMS model based on the above DVMS and RANS models :

$$\begin{gathered}\left(\frac{\partial \overline{W}_h}{\partial t}, \chi_i\right) + \left(\nabla \cdot F(\overline{W}_h), \chi_i\right) = \\ \left(\nabla \cdot V(\overline{W}_h), \phi_i\right) + \theta \left(\tau^{RANS}(\overline{W}_h), \phi_i\right) + (1-\theta)\left(\tau^{DVMS}(W_h'), \phi_i'\right)\end{gathered} \tag{25}$$

Here W_h denotes the hybrid variable solution of the system above. It appears, with this variationnal approach, a theta function wich means a blending function (values in $[0,1]$), creating a convex combinaison of closures terms of these two turbulence models, and τ^{RANS} contains the closure terms of RANS modelisation.
To define the DDES/DVMS model, it suffice to change the RANS closure term by th DDES one.

6.2 Design of the blending functions

As we can see in the previous section, we must define the hybridation function, wich is in a good agreement with the local application of RANS or LES model. There exist several way to define them :

A- One solution consist to define the following hybridation function :

$$\theta = 1 - f_d\ (1 - \overline{\theta}), \tag{26}$$

Where $f_s \in \{f_{d1}, f_{d2}, f_{d3}\}$ which usually called, the *delayed or shielding function*, the choice of these shielding function depends of the thickness blending you want to apply. In our case :

$$\begin{array}{rcl} f_{d1} & = & 1 - \tanh((8r_d)^3), \\ f_{d2} & = & 1 - \tanh((20r_d)^3), \\ f_{d3} & = & 1 - \tanh((8r_d)^4), \end{array} \tag{27}$$

B- The geometric or zonal approach directly depending on the distance to wall:

$$\theta = f_{geo} = 1 - \tanh(\alpha * d_w^4) \tag{28}$$

Where α is prescribed (depending on the mesh choosen).

C- Original blend :

$$\theta = \overline{\theta} \tag{29}$$

Definition of blends methods

1) We choose a blend method as a function of a ratio of turbulence model values :

$$\overline{\theta} = \tanh(\xi^2) \tag{30}$$

with several way to choose ξ :

a) ratio of the length scale :

$$\xi = \frac{\Delta}{l_{k/\epsilon}} \quad \text{with} \quad l_{k/\epsilon} = \frac{k^{3/2}}{\epsilon} \tag{31}$$

b) ratio of turbulent viscosity :

$$\xi = \frac{\mu_{les}}{\mu_{k/\epsilon}} \tag{32}$$

c) ratio of caracteristic time scale :

$$\xi = \frac{\tau_{les}}{\tau_{k/\epsilon}} \quad \text{with} \quad \tau_{les} = \frac{1}{\sqrt{S:S}} \text{ and } \tau_{k/\epsilon} = \frac{k}{\epsilon} \ . \tag{33}$$

2) We can find, on litterature other blending function, Han *et al.* [13] proposed :

$$\overline{\theta} = \min\left(1, \left[\frac{1-\exp(-\beta L_c/L_k}{1-\exp(-\beta L_i/L_k)}\right]^2\right) \tag{34}$$

with L_c is the local size of tetrahedron and $L_i = \frac{k^{3/2}}{\epsilon}$ is the k-ϵ length scale, $L_k = \left(\frac{\nu^3}{\epsilon}\right)^{1/4}$ and $\beta = 2 \times 10^{-3}$. We call it, Han-Krajnovic blending function.

3) A well known blending function is the blending function introduced by [23] to develop k-ω SST model:

$$\overline{\theta} = \tanh(\xi^2)$$

where

$$\xi = \max\left[\frac{2\sqrt{k}}{0.09\omega y}, \frac{500\nu}{y^2\omega}\right] \tag{35}$$

4) We can define the blend method as a zonal approach considering the length scale of the closure model :

$$\overline{\theta} = \begin{cases} 1 & \text{if} \quad l_{k/\epsilon} < \Delta \\ 0 & \quad otherwise \end{cases} \tag{36}$$

5) Another way is to consider the blending function as a blend method and then we have :

$$\overline{\theta} = f_s \ ; \text{ for } f_s \in \{f_{s1}, f_{s2}, f_{s3}\} \tag{37}$$

6) Finally, we can define a regularisation of a zonal approach, consiting to make a continuous function which is 1 near the geometry and 0 otherwise. Consider V the domain you want $\theta = 0$ then we write $\overline{\theta}$ as the following :

$$\overline{\theta} = 1 - \exp\left(-\frac{1}{2\epsilon} d(r,V)^2\right) \tag{38}$$

where $\epsilon > 0$ and $d(r,V)$ is the distance between r and the set V, if $r \in V$ then $d(r,V) = 0$ and $\overline{\theta} = 0$, else $d(r,V) > 0$ and for a small $\epsilon > 0$:

$$\lim_{\epsilon \to 0^+} \overline{\theta} = 1$$

7 A challenging geometry: the circular cylinder

Though the geometry of a circular cylinder is quite simple, computing the flow past this bluff body remains a challenging benchmark. Indeed, the flow physics changes strongly with the Reynolds number [32] and is characterized by many features: attached flow, separated flow, laminar/turbulence transition, shear layer, recirculation, vortex shedding, among others. On the other hand, the flow separation does not occur due to singularities in the geometry as for square or rectangular cylinders for example, which makes the prediction of circular cylinder flows more difficult.
Among the different regimes that can characterize this flow, we can mention the subcritical, critical and supercritcal regimes (Reynolds number ranges are indicative):

- For Reynolds numbers $300 < Re < 3 \times 10^5$, the flow regime is subcritical: the vortex street downstream the cylinder is fully turbulent and the separation points are laminar with a separation angle less than 90^o.
- For Reynolds numbers $3 \times 10^5 < Re < 3.5 \times 10^5$, the critical regime is reached. The boundary layer is laminar on one side of the cylinder. On the other side, turbulence settles in the attached boundary layer and the separation point is turbulent leading to delayed separation. This results in a sudden drop in drag coefficient known as the *Drag crisis*. The wake is narrower and disorganized, and no vortex street is apparent.
- For Reynolds numbers $3.5 \times 10^5 < Re < 3.5 \times 10^6$, the flow regime is supercritical: the boundary layer is turbulent on both sides of the cylinder when the flow separates, which results in a separation located further downstream compared to the subcritical case (separation angle greater than 90^o). The turbulent vortex street reappears and the wake is thinner. The drag coefficient increases while remaining lower than the values observed in subcritical regime.

7.1 Reynolds =140K

The conditions of computation for this subcrittcal case are as follows:

- **Computational grids:**
  0.892MNodes span= 2D
  165x165x21 mesh
- **Flow parameters:**
  361x325x3 mesh
  112000 times steps
  cfl= 40
  better ageement with experiments that 165x165x3 mesh

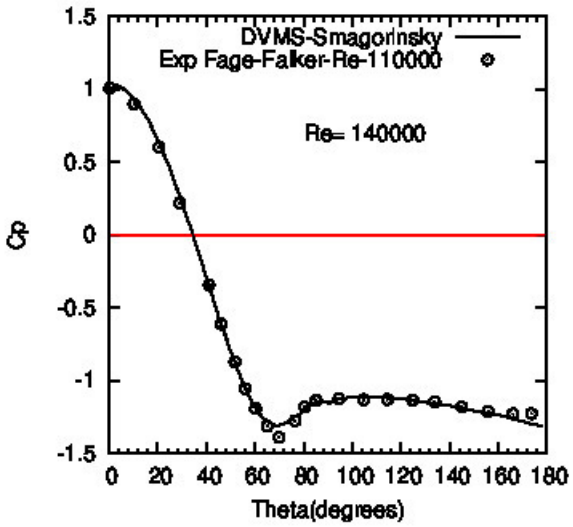

Figure 3: Cylinder at Reynolds number 140K. Computation with the option DVMS-Smagorinsky. Coarse mesh 165×165. The experimental curve was published in [5].

	mesh	$\overline{C}_d$	$-\overline{C}_{p_b}$	L_r	S_t
Experiments					
Cantwell-Coles (1983)		1.24	1.21	0.5	0.179
Son-Hanratty (1969)					$\simeq 0.2$
Zdravkovich (1997)					$\simeq 0.2$
Present simulations					
No model	165x165	0.43	0.40	0.63	0.142
URANS $k-\varepsilon$	165x165	0.77	0.87	1.05	0.218
DDES $k-\varepsilon$	165x165	0.97	1.01	0.96	0.217
DDES/DVMS	165x165	1.04	1.12	0.91	0.214
DVMS	165x165	1.25	1.33	0.88	0.217
DVMS	361x325	1.32	1.17	0.56	0.166

Table 1: Bulk quantities for $Re = 140,000$ flow around a cylinder.

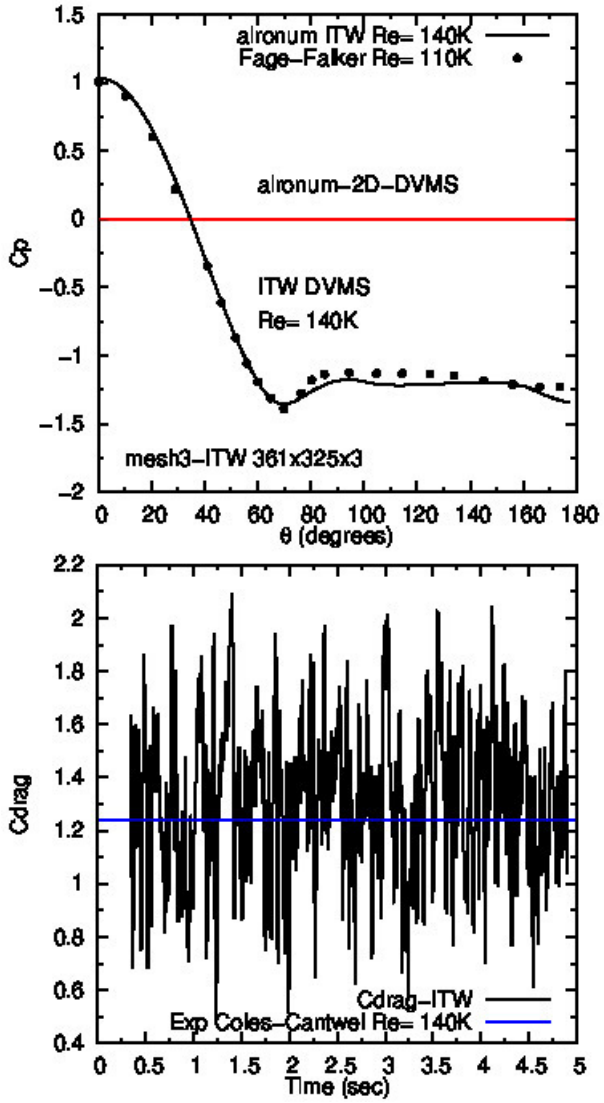

Figure 4: Cylinder at Reynolds number 140K. Computation with the option DVMS-Smagorinsky. Finer mesh 361×325. The experimental curve was published in [5].

7.2 Reynolds =1M

Let us start this part devoted to hybrid calculations by presenting the results of a circular cylinder flow at Reynolds number, based on the cylinder diameter D and on the freesream velocity, equal to 1 million. The computational domain is such that $-15 \leq x, y \leq 15$, and $-1 \leq z \leq 1$ where x, y and z denote the streamwise, transverse and spanwise directions respectively, the cylinder axis being located at $x = y = z = 0$. The mesh involves 4.8 millions nodes and 6.8 millions tetrahedra. In this study, the Reichardt wall law (1) is used. Moreover, the subgrid scale model used for hybrid model is either Smagorinsky or WALE model (mentioned in tables) in their dynamic version. The hybrid function is chosen of the form of (24) with $f_s = f_{s_1}$ and $\overline{\theta}$ designed as (28) with (29).

Only a few results with Reynolds larger than 5×10^5 are available in the litterature. This range corresponds to a supercritical regime for which the boundary layer is turbulent at the flow separation. It is generally admitted that the vortex shedding strength is low over the interval $[5 \times 10^5, 1.5 \times 10^6]$. Experimental results involve those of Shih *et al.* [25], Schewe [24], Guven *et al.* [12], Goelling [9] and Zdravkovich [31]. Computations are even more difficult to find in the literature. LES computations of Kim et Mohan [17], Catalano *et al.* [3], Ono and Tamura [22], and RANS computations of Catalano *et al.* [3] are used for comparison purpose. These simulations were performed with grids of 2.3×10^6 nodes (Catalano *et al.* [3]), 4.5×10^6 nodes (Ono and Tamura [22]) and 6.8×10^6 nodes (Kim and Mohan [17]). Probably LES computations performed with less than 4 million nodes are underresolved and produce in particular a too large drag.

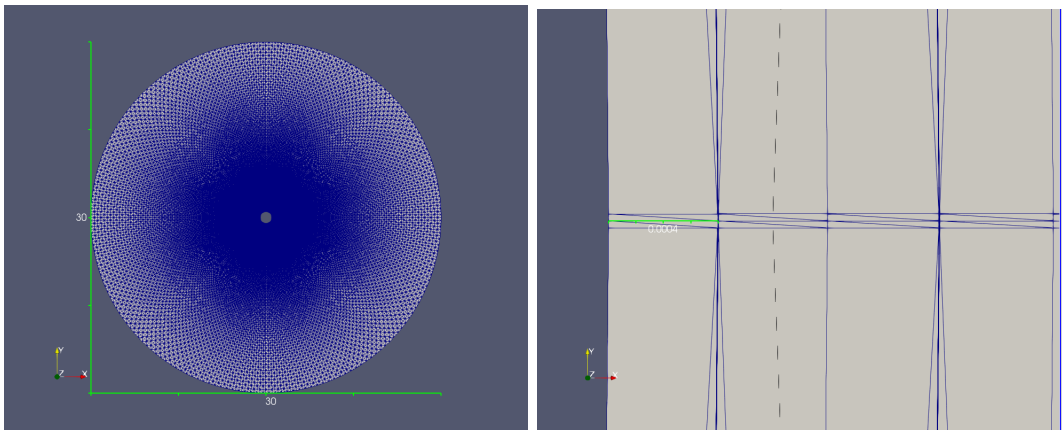

Figure 5: Computational domain

Name	Mesh size	y_w^+	y_m^+	$\overline{C}_d$	C_l'	$-\overline{C}_{pb}$	L_r	$\overline{\theta}$
Experiments								
Shih et *al* [25]				0.24	-	0.33		
Schewe [24]				0.22	-	-		
Szechenyi [29]				0.25	-	0.32		
Glling [9]							-	130
Zdravkovich [31]				0.2-0.4	0.1-0.15	0.2-0.34		
Other simulations								
RANS Catalano [3]	2.3M	-	-	0.39	-	0.33		
LES Catalano [3]	2.3M	-	-	0.31	-	0.32		
LES Ono [22] Re=600K	4.5M	-	-	0.27	0.13		-	
LES Kim [17]	6.8M	-	-	0.27	0.12	0.28	-	108
Present simulations								
URANS								
URANS $k-\varepsilon$	-	-	-	0.24	0.07	0.26	-	-
DDES								
DDES $k-\varepsilon$ Goldberg WL	4.8M	20	100	0.20	0.04	0.22	0.87	138
DDES $k-\varepsilon$ Goldberg WL	4.8M	20	25	0.40	0.05	0.56	1.46	113
DDES $k-\varepsilon$ Goldberg ITW	4.8M	1	-	0.50	0.07	0.54	1.22	103
DDES/ DVMS								
k - ε / cubic WL Smagorinsky	4.8M	20	100	0.20	0.02	0.22	0.82	135
k - ε / cubic WALE ITW	4.8M	1	-	0.49	0.06	0.60	1.56	104
RANS / DVMS								
k - ε / cubic Smagorinsky WL	4.8M	20	100	0.24	0.05	0.22	0.62	133
k - ε / Shur WALE WL	4.8M	1	100	0.25	0.11	0.23	0.68	133
k - ε / cubic WALE ITW	4.8M	1	-	0.48	0.11	0.55	1.14	109

Table 2: Bulk coefficient of the flow around a circular cylinder at Reynolds number 1M, $\overline{C}_d$ holds for the mean drag coefficient, C_l' is the root mean square of lift time fluctuation, $\overline{C}_{p_b}$ is the pressure coefficient at cylinder basis, L_r is the mean recirculation lenght, $\overline{\theta}$ is the mean separation angle.

From these results, we notice in Table 2 that RANS/DVMS model is better than others, in particular the drag coefficient is contained in Zdravkovich [31] interval for the wall law modelisation and also in a very good agreement with others experiments. But lift root mean square is under estimated for all simulations compared to experimental datas, however we observe that it is not the case for integration to the wall modelisation. In the other hand, the predicted mean separation angle, which correspond to a turbulent flow separation, is closed to experimental data for the wall law, the DDES and hybrids DDES are over estimated and under estimated for all in the case of ITW.

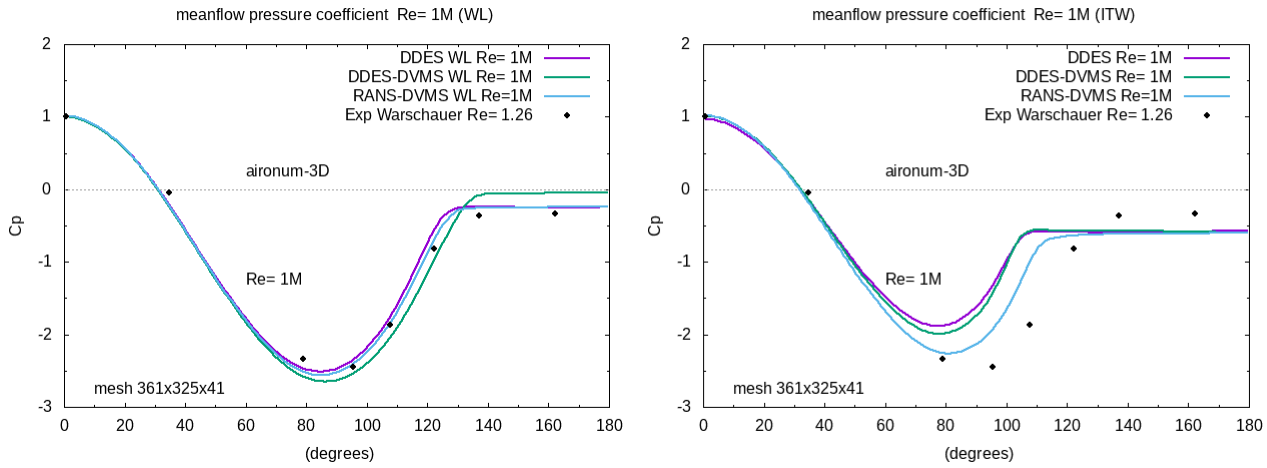

Figure 6: Distribution of mean pressure as a function of polar angle. Comparaison between experiment. Wall law on the left and integration to the wall on the right.

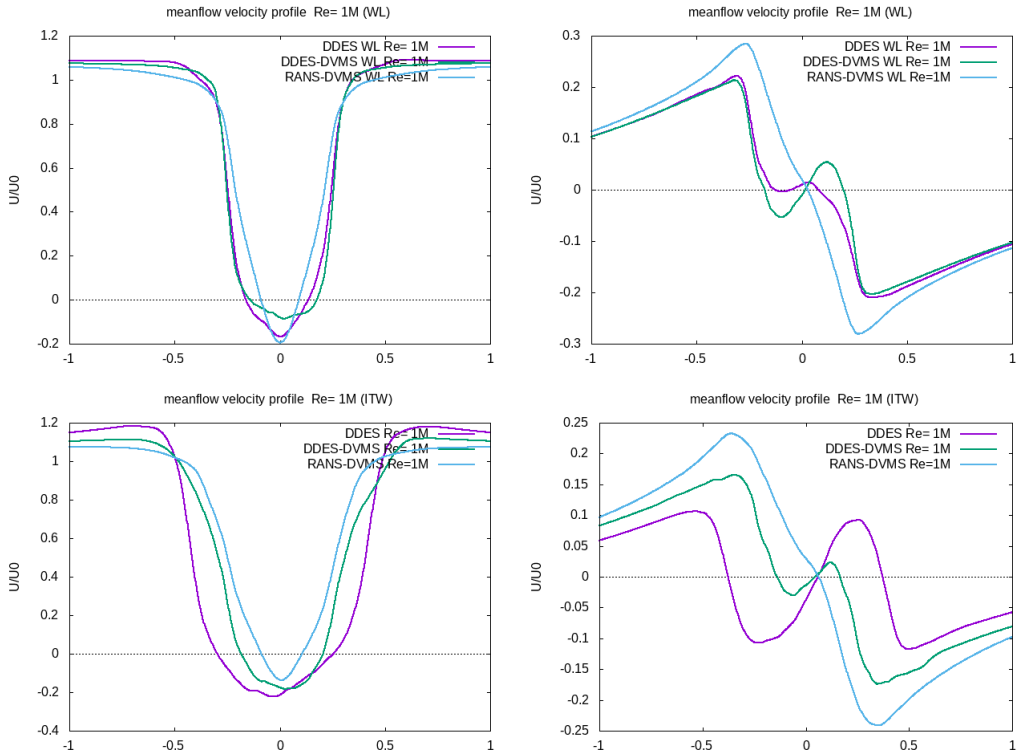

Figure 7: On the top longitudonal velocity profile at $x/D = 1$, and on bottom the transverse velocity.

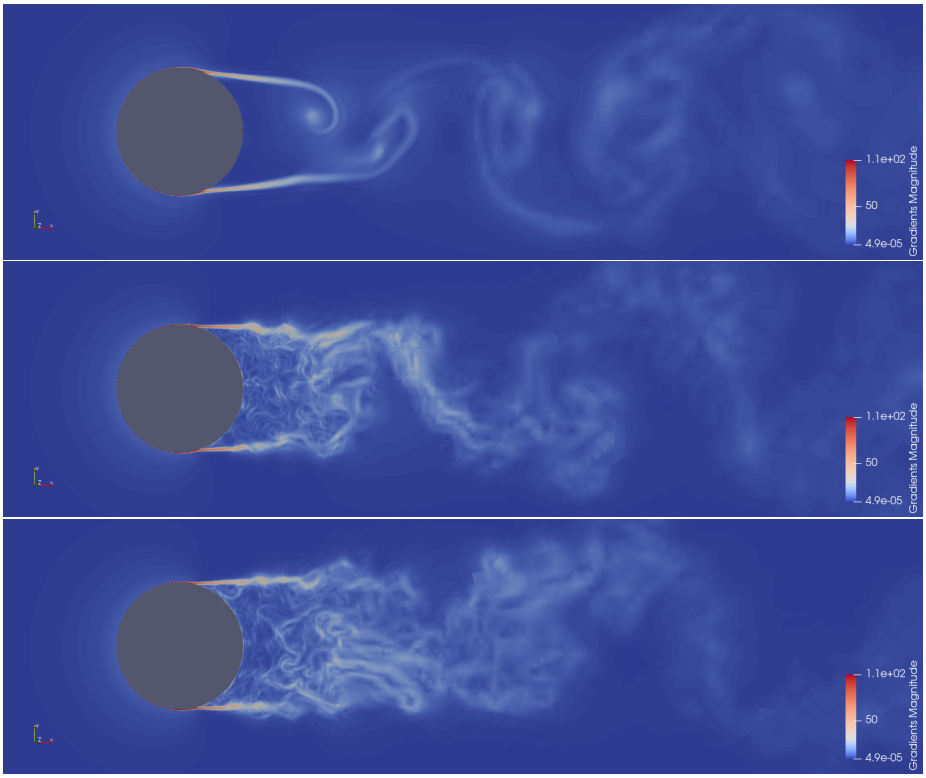

Figure 8: Instantaneous vorticity field of our models at Reynolds 1 million. From top to bottom: /RANS-DVMS-ITW, DDES-ITW, DDES-DVMS-ITW

7.3 Reynolds =2M

The computational grids are either quasi 2D or fully 3D:
- 2D: Inria 361x325 structured,
- 3D: Inria 4.8MNodes 361x325x41 structured, span = 2D and 3D.
We also refer to results obtained by KIAM's 3D unstructured mesh with 4.8MNodes.

Figure 9 compares the aironum URANS-WL surface pressure with the recent paper of Sreenivasan(2019), both are two-dimensional computations [1]. Figure 9 shows that AIRONUM correctly predicts the minimum Cp surface pressure using a WL. That the WL gives accurate surface pressure on the cylinder should not be surprising as experiments show that turbulent separation occurs and the flow is fully turbulent at Re= 1M and 2M.

Figure 10 compares the aironum URANS-WL and URANS-ITW surface pressures. We would like better agreement between the WL and ITW results. To explain the lack of agreement we note that 1) The WL requires no transition model as the flow is assumed to be full turbulent whereas 2) ITW requires a transition model (under development in the AIRONUM software) and 3) ITW is more sensitive to the mesh than the WL,requiring a very fine mesh near the no-slip surface.

[1]Other than [3], who only gave Cd values, the author could find no other published 3D CFD results at Re= 2M with which to compare the present results.

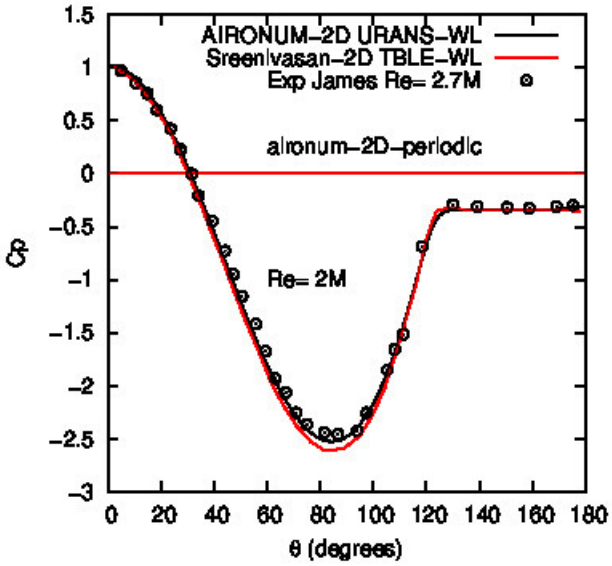

Figure 9: Cylinder at Reynolds number 2M. Surface pressure using a WL. Experiment at Reynolds number 2.7M comes from [16]

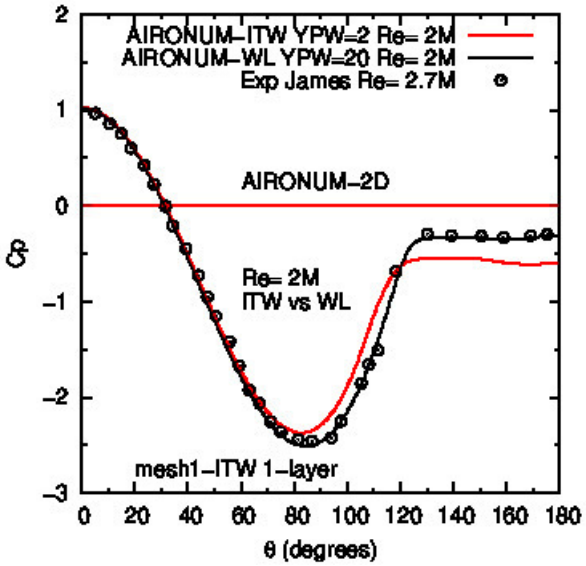

Figure 10: Cylinder at Reynolds number 2M. Surface pressure- WL vs ITW. Experiment at Reynolds number 2.7M comes from [16].

It is difficult to discuss the Re= 2M results without comparison with the Re= 1M results. Shown in Figure 11, for the WL case, are the lift spectra for both Reynolds numbers compared with the Kolmogorov energy scale. The excellent agreement with the Kolmogorov scale gives confidence that the meshes used are sufficient for the WL. The probe was located at (x,y,z) = (1,0,0).

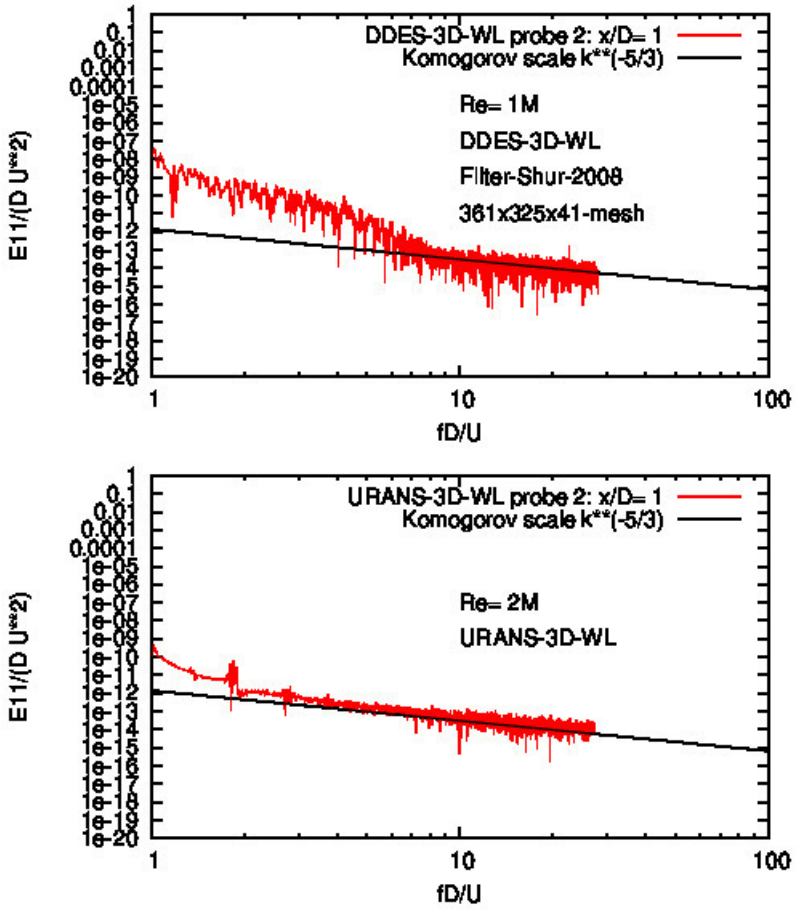

Figure 11: Lift Spectra at Re= 1M and Re- 2M.

Re= 2M	mesh/Re	model/Δ SGS filter	$\overline{C_d}$	C_l'	-Cp_b	$\overline{\theta}$	St/VTC
Exp Shih et al.	Re= 1.5M		0.26	0.033	0.40	105	0.46
Exp Schewe al.	Re= 2.0M		0.32	0.029	na	na	0.26
2D-WL							
AIRONUM-2D	Inria2D	RANS-WL	0.19	-	0.23	124	-/-
AIRONUM-2D	Inria2D	URANS-WL	0.29	0.12	0.30	115	0.41
Sreenivasan-2D	Grid2D	TBLE-WL	0.24	0.029	0.36	105	0.36
3D-WL							
AIRONUM-3D	Inria3D	DDES-WL/Δ_{Shur}	0.28	0.038	0.27	132	0.42/108
AIRONUM-3D	Inria3D	URANS-DVMS-WL	0.26	0.048	0.31	128	0.44
AIRONUM-3D	Inria3D	URANS-WL	0.26	0.066	0.30	128	0.42/26
3D-ITW							
NOISEtte-3D	KIAM3D-f	DDES-ITW/Δ_{SLA}	0.23	0.051	0.58	110	0.315
NOISEtte-3D	KIAM3D-c	DDES-ITW/Δ_{SLA}	0.22	0.027	0.55	109	0.34

Table 3: Re= 2M: $\bar{C_d}$ is the mean drag, $C_l^{'}$ is the root mean square (r.m.s) of the lift coefficient, $\bar{\theta}$ is the mean flow separation angle. St is the Strouhal number based on the diameter, $\overline{L_r}/D$ the mean flow recirculation length. Grid-2D 3.3M elements. Inria2D mesh has 117K vertices structured. Inria3D mesh has 4.8M vertices structured. KIAM3D-c mesh 4.48M unstructured.

Correctly predicts CL'_{rms}			
Re	2D	3D	Notes
1M	yes-WL	yes-WL	exceptions: Moussaed(2013,2014)and Kim and Mohan(2005)
2M	no-WL	yes-WL	
1M	no-ITW	yes-ITW	
2M	no-ITW	no-ITW	

Table 4: Prediction of CL'_{rms} at Re= 1M and Re= 2M

8 Cylinder Re= 1M and 2M: Summary WL results

Table 3 shows various results for the Re= 2M case from which the following are noted.

- Observations at Re= 2M : LES, DDES and other Hybrid methods using a WL :
  - The focus here is on the prediction of CL'.
  - AIRONUM-2D over-predicts the experimental CL' values at Re= 2M.
  - Sreenivasan's TBLE-2D correctly predicts the experimental CL' values at Re= 2M. ✓
  - AIRONUM-3D correctly predicts the experimental CL' values at Re= 2M. ✓
  - No published 3D CFD detailed studies exist with which to compare.

- Observations at Re= 1M :
  - TBLE-2D and AIRONUM-2D correctly predict the experimental CL' value at Re= 1M. ✓
  - Moussaed(2013,2014) correctly predicted the exp CL' value at Re= 1M. ✓
  - Kim and Mohan(2005) correctly predicted the exp CL' value at Re= 1M. ✓
  - AIRONUM-3D correctly predicts the experimental CL' value at Re= 1M.
  - With the exception of Moussaed (2013), Moussaed et al.(2014) and, Kim and Mohan(2005), no published 3D CFD results exist that correctly predict the experimental CL' values at Re= 1M.

Table 4 summarizes the status of the Re= 1M and Re= 2M test cases.

9 Concluding remarks

The $Rey = 140$K case remains a difficult case due to the high variations of bulk coefficicents appearing when the mesh is refined.

The $Rey = 1$M case is computed with the different options and results are reasonably accurate.

Concerning the $Rey = 2$M case, some tracks to explore are:
- AIRONUM, add a transition prediction model in order to more accurately compute transitional boundary layers (ITW, supercritical regime).
$k-R$ transition model (Zhang-Rahman-Chen, 2019) combined with DDES, URANS/DVMS and DDES/DVMS.
- It is necessary to validate the Δ_{SLA} (shear-layer-adaptive) filter in the AIRONUM sortware. - A SST $k-\omega$ model could be combined with DDES, RANS/DVMS and DDES/DVMS.
- We have to further improve the blending function in the URANS/DVMS approach.
- A seamless DDES/DVMS strategy based on a blending function allowing for an automatic switch from DDES to DVMS and vice versa has to be found.
- A DDES variant (limitation of the production term, Reddy-Ryon-Durbin, 2014) which avoids the log-layer mismatch issue should be derived.

Acknowledgements

This work was supported by the ANR NORMA project, grant ANR-19-CE40-0020-01 of the French National Research Agency. The authors gratefully acknowledge GENCI for granted access to HPC resources through CINES (grant 2020-A0092A05067).

REFERENCES

[1] R. El Akoury. *Analyse physique des effets de rotation de paroi en coulements transitionnels et modlisation d'coulements turbulents autour de structures portantes.* PhD thesis, INPT, Toulouse, France, 2007. (in French).

[2] S. Camarri, B. Koobus, M. V. Salvetti, and A. Dervieux. A low-diffusion MUSCL scheme for LES on unstructured grids. *Computers and Fluids*, 33:1101–1129, 2004.

[3] P. Catalano, Meng Wang, G. Iaccarino, and P. Moin. Numerical simulation of the flow around a circular cylinder at high Reynolds numbers. *Int. J. Heat Fluid Flow*, 24:463–469, 2003.

[4] C. Debiez and A. Dervieux. Mixed element volume muscl methods with weak viscosity for steady and unsteady flow calculation. *Computer and Fluids*, 29:89–118, 1999.

[5] A. Fage and V.M. Falkner. Further experiments on the flow around a cylinder. *Aeronautical research committee reports and memoranda*, 1369:1–25, 1931.

[6] C. Farhat, A. Rajasekharan, and B. Koobus. A dynamic variational multiscale method for large eddy simulation on unstructured meshes. *Computer Methods in Applied Mathematics and Engineering*, 195:1667–1667, 2006.

[7] J. Francescatto, A. Dervieux, and M. Ravachol. Efficiency of the Menter correction for steady and unsteady non smooth flows. In T.W.J. Peeters K. Hanjalic, editor, *Proceedings of the Second international Symposium on Turbulence Heat and Mass Transfer, Delft, The Netherlands*, pages 399–408. Delft University Press, 1997.

[8] M. Germano, U. Piomelli, P. Moin, and W.H. Cabot. A dynamic subgrid-scale eddy viscosity model. *Phys. Fluids*, A 3:1760–1765, 1991.

[9] B. Goelling. Experimental investigations of separating boundary-layer flow from circular cylinder at Reynolds numbers from 10^5 up to 10^7; three-dimensional vortex flow of a circular cylinder. In G.E.A. Meier and K.R. Sreenivasan, editors, *Proceedings of IUTAM Symposium on One Hundred Years of Bloundary Layer Research*, pages 455–462, The Netherlands, 2006. Springer.

[10] U. Goldberg, O. Peroomian, and S. Chakravarthy. A wall-distance-free $k-\varepsilon$ model with enhanced near-wall treatment. *Journal of Fluids Engineering*, 120:457–462, 1998.

[11] M.S. Gritskevich, A.V. Garbaruk, J. Schultze, and F.R. Menter. Development of DDES and IDDES formulations for the $k-\omega$ shear stress transport model. *Flow, Turbul. Combust.*, 88:431449, 2012.

[12] O. Guven, C. Farell, and V.C. Patel. Surface-roughness effects on the mean flow past circular cylinders. *J. Fluid Mech.*, 98(4):673–701, 1980.

[13] X. Han and S. Krajnović. An efficient very large eddy simulation of turbulent flow. *Int. J. Numer. Meth. Fluids*, 71:1341–1360, 2013.

[14] J. Holmen, T.J.R. Hughes, A.A. Oberai, and G.N. Wells. Sensitivity of the scale partition for variational multiscale large-eddy simulation of channel flow. *Physics of Fluids*, 16(3):824–827, 2004.

[15] E. Itam, S. Wornom, B. Koobus, and A. Dervieux. Application of a hybrid variational multiscale model to massively separated flows. *3AF, Toulouse, France*, 2015.

[16] W.D. James, S.W. Paris, and G.V. Malcolm. Study of viscous cross flow effects on circular cylinders at high Reynolds numbers. *AIAA Journal*, 18:1066–1072, 1980.

[17] S.-E. Kim and L.S. Mohan. Prediction of unsteady loading on a circular cylinder in high reynolds number flows using large eddy simulation. *Proceedings of OMAE 2005: 24th International Conference on Offshore Mechanics and Artic Engineering, june 12-16, Halkidiki, Greece, OMAE 2005-67044*, 2005.

[18] B. Koobus and C. Farhat. A variational multiscale method for the large eddy simulation of compressible turbulent flows on unstructured meshes-application to vortex shedding. *Computer Methods in Applied Mechanics and Engineering*, 193:1367–1383, 2004.

[19] M.H. Lallemand, H. Steve, and A. Dervieux. Unstructured multigridding by volume agglomeration: current status. *Comput. Fluids*, 21:397–433, 1992.

[20] D.K. Lilly. A proposed modification of the Germano subgrid-scale closure method. *Phys. Fluids*, A4:633, 1992.

[21] F. Nicoud and F. Ducros. Subgrid-scale stress modelling based on the square of the velocity gradient tensor. *Flow Turbulence and Combustion*, 62(3):183–200, 1999.

[22] Y. Ono and T. Tamura. LES of flows around a circular cylinder in the critical Reynolds number region. In *Proceedings of BBAA VI International Colloquium on Bluff Bodies Aerodynamics and Applications*, Milano, Italy, July 20-24 2008.

[23] Menter F. R. Two-equation eddy-viscosity turbulence models for engineering applications. *AIAA J.*, 32:1598–1605, 1994.

[24] G. Schewe. On the force fluctuations acting on a circular cylinder in crossflow from subcritical up to transcritical Reynolds numbers. *Journal of Fluid Mechganics*, 133:265–285, 1995.

[25] W.C.L. Shih, C. Wang, D. Coles, and A. Roshko. Experiments on flow past rough circular cylinders at large Reynolds numbers. *J. Wind Eng. Indust. Aerodyn.*, 49:351–368, 1993.

[26] J. Smagorinsky. General circulation experiments with the primitive equations. *Monthly Weather Review*, 91(3):99–164, 1963.

[27] P.R. Spalart, W.H. Jou, M. Strelets, and S. Allmaras. *Advances in DNS/LES*, chapter Comments on the feasibility of LES for wings and on a hybrid RANS/LES approach. Columbus (OH), 1997.

[28] C.G. Speziale. A combined large-eddy simulation and time-dependent RANS capability for high-speed compressible flow. *Journal of Scientific Computing*, 13(3):253–274, 1998.

[29] E. Szechenyi. Supercritical Reynolds number simulation for two-dimensional flow over circular cylinders. *J. Fluid Mech.*, 70:529–542, 1975.

[30] H. Baya Toda, K. Truffin, and F. Nicoud. Is the dynamic procedure appropriate for all SGS model. In J.F.C. Pereira and A. Sequeira, editors, *Proceedings of the V European Conference on Computational Fluid Dynamics, ECCOMAS CFD 2010 Lisbon, Portugal*, 2010.

[31] M. M. Zdravkovich. Different modes on vortex shedding: an overview. *Journal of Fluid and Structures*, 10(5):427–437, 1996.

[32] M.M. Zdravkovitch. *Flow around Circular Cylinders Vol 1: Fundamentals*. Oxford University Press, 1997.